

Simulation of molecular ring emission spectra: localization of exciton states and dynamics

David Zapletal, Pavel Heřman

Abstract—Computer simulation of steady state fluorescence spectra of the ring molecular system is presented in this paper. The cyclic antenna unit LH2 of the bacterial photosystem from purple bacterium *Rhodospseudomonas acidophila* can be modeled by such system. Three different models of uncorrelated static disorder are taking into account in our simulations: Gaussian disorder in local excitation energies, Gaussian disorder in nearest neighbour transfer integrals and Gaussian disorder in radial positions of molecules in the ring. Dynamic disorder, interaction with a bath, is also included in Markovian approximation. The cumulant-expansion method of Mukamel et al. is used for the calculation of spectral responses of the system with exciton-phonon coupling. The peak position of single ring spectra and localization of exciton states depend on realization of static disorder and is also influenced by dynamic disorder. We discuss different types of exciton dynamics too, that are coupled to above mentioned effects and compare the results in that the dynamic disorder is taken into account with the results without dynamic disorder.

Keywords—Dynamic disorder, exciton states, fluorescence spectrum, LH2, *Mathematica*, static disorder.

I. INTRODUCTION

In 1995 the crystal structure of peripheral light-harvesting complex LH2 from purple bacterium *Rhodospseudomonas acidophila* was determined with high resolution [1], [2]. That is why ultrafast initial phases of photosynthesis in purple bacteria could be thoroughly studied in last two decades. LH2 is a highly symmetric antenna complex in which a very efficient light collection and excitation transfer through the LH1 units towards the reaction center takes place. LH2 complex consists of nine pigment-protein subunits, each containing two transmembrane polypeptide helices

and three bacteriochlorophylls (BChl). The B850 ring in LH2 is composed of nine repeating dimer pairs of BChl molecules with nearly tangentially oriented transition dipole moments.

Due to the strong interaction between BChl molecules, an extended Frenkel exciton states model is considered in our theoretical approach. In spite of extensive investigation, the role of the protein moiety in governing the dynamics of the excited states has not been totally clear yet. At room temperature the solvent and protein environment fluctuate with characteristic time scales ranging from femtoseconds to nanoseconds. The dynamical aspects of the system are reflected, e.g., in the lineshapes as well as in the time dependence of the optical properties. To fully characterize the line shape of an optical transition and thereby the dynamics of the system, one needs to know not only the fluctuation amplitude but also the time scale of each process involved. The observed linewidth reflect the combined influence of static disorder and exciton coupling to intermolecular, intramolecular and solvent nuclear motions. The simplest approach is to substitute fast fluctuations by dynamic disorder and slow fluctuations by static disorder.

For zero disorder the exciton manifold features two non-degenerate and eight pairwise degenerate states. In the presence of the energetic disorder the degeneracy of the exciton states is lifted and oscillator strength is redistributed among the exciton states.

Kumble, Hochstrasser [3] and Nagarajan et al. [4]–[6] studied static disorder effect on the anisotropy of fluorescence for LH2 rings. We have extended these investigations by consideration of dynamic disorder. We have scrutinized the Redfield equations with a secular approximation which have been generally used to describe the system bath interaction with a weak exciton-bath interaction. We have found that use of secular approximation distorts true time development of the exciton transfer. After studying the influence of dynamic disorder for simple systems (dimer, trimer) [7]–[9] we added this effect to our model of LH2 ring by using a quantum master equation in the Markovian [10] and non-Markovian limits [11].

Break up of the coherent exciton transfer regime is indicated in the time dependence of the anisotropy of fluorescence by its drop from 0.7 to 0.4. It has been shown that non Markovian approach in taking interaction with the bath into account leads to retardation and slower

Manuscript received December 2, 2011. Revised version received

.....
This work was supported in part by the Faculty of Science, University of Hradec Králové (project of specific research No. 2116/2011 - P. Heřman).

D. Zapletal is with the Institute of Mathematics, Faculty of Economics and Administration, University of Pardubice, Studentská 95, 53210 Pardubice, Czech Republic (e-mail: david.zapletal@upce.cz).

P. Heřman is with the Department of Physics, Faculty of Science, University of Hradec Králové, Rokitsanského 62, 50003 Hradec Králové, Czech Republic (e-mail: pavel.herman@uhk.cz).

decrease of the anisotropy of fluorescence [11], [12]. Influence of four types of uncorrelated static disorder [12], [13] and correlated static disorder (elliptical deformation) [11] was investigated. We also compared models of rings with different arrangement of optical dipole moments (radial arrangement) [14]–[16].

Recently we have focused on the modeling of the steady state fluorescence and absorption spectra for above mentioned model of LH2 ring [17]. Main goal of the present paper is the investigation of different types of exciton dynamics, that are coupled to exciton states with different degree of localization. The dynamic disorder - interaction with the phonon bath in Markovian approximation is taken into account simultaneously with uncorrelated static disorder.

Present paper is the extension of our contribution [18] presented on WSEAS conference MACMESE'11. The rest of the paper is structured as follows. Section II. introduces the ring model with three types of uncorrelated static disorder and the cumulant expansion method of Mukamel et al. [20], [21], which is used for the calculation of spectral responses of the system with exciton-phonon coupling. In Section III. the computational point of view for our calculations is discussed. The graphically presented results of our simulations and used units and parameters could be found in Section IV. In Section V. some conclusions are drawn.

II. PHYSICAL MODEL

The Hamiltonian of an exciton in the ring coupled to a bath of harmonic oscillators reads

$$H = H_{\text{ex}}^0 + H_{\text{ph}} + H_{\text{ex-ph}} + H_{\text{s}}^x. \quad (1)$$

Here the first term,

$$H_{\text{ex}}^0 = \sum_{m,n(m \neq n)} J_{mn} a_m^\dagger a_n, \quad (2)$$

corresponds to an exciton, e.g. the system without any disorder (the operator a_m^\dagger (a_m) creates (annihilates) an exciton at site m), J_{mn} (for $m \neq n$) is the so-called transfer integral between sites m and n .

The second term,

$$H_{\text{ph}} = \sum_q \hbar \omega_q b_q^\dagger b_q, \quad (3)$$

represents phonon bath in the harmonic approximation (the phonon creation and annihilation operators are denoted by b_q^\dagger and b_{-q} , respectively).

Third term in (1),

$$H_{\text{ex-ph}} = \frac{1}{\sqrt{N}} \sum_m \sum_q G_q^m \hbar \omega_q a_m^\dagger a_m (b_q^\dagger + b_{-q}), \quad (4)$$

describes exciton-phonon interaction which is assumed to be site-diagonal and linear in the bath coordinates (the

term G_q^m denotes the exciton-phonon coupling constant). Last term in (1), H_{s}^x , corresponds to static disorder. Influence of static disorder is modeled by a Gaussian distribution:

- (I) for the uncorrelated local excitation energy fluctuations $\delta \varepsilon_n$ with the standard deviation Δ

$$H_{\text{s}}^I = \sum_n \delta \varepsilon_n a_n^\dagger a_n, \quad (5)$$

- (II) for the uncorrelated transfer integral fluctuations δJ_{mn} with the standard deviation Δ_J (nearest neighbour approximation)

$$H_{\text{s}}^{II} = \sum_{mn(m \neq n)} \delta J_{mn} a_m^\dagger a_n, \quad (6)$$

- (III) for the uncorrelated fluctuations of radial positions of molecules on the ring δr_n with the standard deviation Δ_r

$$r_n = r_0 + \delta r_n, \quad (7)$$

where r_0 is the radius of unperturbed ring.

Inside one ring the pure exciton Hamiltonian can be diagonalized using the wave vector representation with corresponding delocalized "Bloch" states α and energies E_α . Considering homogeneous case with only nearest neighbour transfer matrix elements

$$J_{mn} = J_0(\delta_{m,n+1} + \delta_{m,n-1}) \quad (8)$$

and using Fourier transformed excitonic operators (Bloch representation)

$$a_\alpha = \sum_n e^{i\alpha kn}, \quad (9)$$

where

$$\alpha = \frac{2\pi}{N} l, \quad l = 0, \pm 1, \dots, \pm \frac{N}{2}, \quad (10)$$

the simplest exciton Hamiltonian in α - representation reads

$$H_{\text{ex}}^0 = \sum_\alpha E_\alpha a_\alpha^\dagger a_\alpha, \quad (11)$$

with

$$E_\alpha = -2J_0 \cos \alpha. \quad (12)$$

The cumulant-expansion method of Mukamel et al. [20], [21] is used for the calculation of spectral responses of the system with exciton-phonon coupling. Absorption $OD(\omega)$ and steady-state fluorescence $FL(\omega)$ spectrum can be expressed as

$$OD(\omega) = \omega \sum_\alpha d_\alpha^2 \times \times \text{Re} \int_0^\infty dt e^{i(\omega - \omega_\alpha)t - g_{\alpha\alpha\alpha\alpha}(t) - R_{\alpha\alpha\alpha\alpha}t}, \quad (13)$$

$$FL(\omega) = \omega \sum_\alpha P_\alpha d_\alpha^2 \times$$

$$\times \text{Re} \int_0^\infty dt e^{i(\omega - \omega_\alpha)t + i\lambda_{\alpha\alpha\alpha\alpha}t - g_{\alpha\alpha\alpha\alpha}^*(t) - R_{\alpha\alpha\alpha\alpha}t}. \quad (14)$$

Here

$$\vec{d}_\alpha = \sum_n c_n^\alpha \vec{d}_n \quad (15)$$

is the dipole strength of eigenstate α , c_n^α are the expansion coefficients of the eigenstate α in site representation and P_α is the steady state population of the eigenstate α . The inverse lifetime of exciton state $R_{\alpha\alpha\alpha\alpha}$ [19] is given by the elements of Redfield tensor [22] (a sum of the relaxation rates between exciton states)

$$R_{\alpha\alpha\alpha\alpha} = - \sum_{\beta \neq \alpha} R_{\beta\beta\alpha\alpha}. \quad (16)$$

The g-function and λ -values in (14) are given by

$$g_{\alpha\beta\gamma\delta} = - \int_{-\infty}^\infty \frac{d\omega}{2\pi\omega^2} C_{\alpha\beta\gamma\delta}(\omega) \times \left[\coth \frac{\omega}{2k_B T} (\cos \omega t - 1) - i(\sin \omega t - \omega t) \right], \quad (17)$$

$$\begin{aligned} \lambda_{\alpha\beta\gamma\delta} &= - \lim_{t \rightarrow \infty} \frac{d}{dt} \text{Im} \{ g_{\alpha\beta\gamma\delta}(t) \} = \\ &= \int_{-\infty}^\infty \frac{d\omega}{2\pi\omega} C_{\alpha\beta\gamma\delta}(\omega). \end{aligned} \quad (18)$$

The matrix of the spectral densities $C_{\alpha\beta\gamma\delta}(\omega)$ in the eigenstate (exciton) representation reflects one-exciton states coupling to the manifold of nuclear modes. In what follows only a diagonal exciton phonon interaction in site representation is used (see (4)), i.e., only fluctuations of the pigment site energies are assumed and the restriction to the completely uncorrelated dynamical disorder is applied. In such case each site (i.e. each chromophore) has its own bath completely uncoupled from the baths of the other sites. Furthermore, it is assumed that these independent baths have identical properties [12], [23], [24]

$$C_{mm'm'n'}(\omega) = \delta_{mn} \delta_{mm'} \delta_{nn'} C(\omega). \quad (19)$$

After transformation to exciton representation we have

$$C_{\alpha\beta\gamma\delta}(\omega) = \sum_n c_n^\alpha c_n^\beta c_n^\gamma c_n^\delta C(\omega). \quad (20)$$

Several models of spectral density of the bath are used in literature [19], [25], [26]. In our present investigation we have used the model of Kühn and May [25]

$$C(\omega) = \Theta(\omega) j_0 \frac{\omega^2}{2\omega_c^3} e^{-\omega/\omega_c} \quad (21)$$

which has its maximum at $2\omega_c$.

Delocalization of the exciton states contributing to the steady state FL spectrum can be characterized by the thermally averaged participation ratio $\langle PR \rangle$, which is given by

$$\langle PR \rangle = \frac{\sum_\alpha PR_\alpha e^{-\frac{E_\alpha}{k_B T}}}{\sum_\alpha e^{-\frac{E_\alpha}{k_B T}}}, \quad (22)$$

with

$$PR_\alpha = \sum_{n=1}^N |c_n^\alpha|^4. \quad (23)$$

Time evolution of exciton density matrix $\rho_{\alpha\beta}$ is governed by Redfield equation [22],

$$\frac{\partial \rho_{\alpha\beta}(t)}{\partial t} = -i\omega_{\alpha\beta} \rho_{\alpha\beta}(t) + \sum_{\gamma\delta} R_{\alpha\beta\gamma\delta} \rho_{\gamma\delta}(t), \quad (24)$$

which is equivalent to Čápek's equation [12]. Exciton density matrix in site representation is given by

$$\rho_{mn} = \sum_{\alpha\beta} c_n^\alpha c_n^\beta \rho_{\alpha\beta}. \quad (25)$$

III. COMPUTATIONAL POINT OF VIEW

To have steady state fluorescence spectrum $FL(\omega)$ and absorption spectrum $OD(\omega)$, it is necessary to calculate single ring $FL(\omega)$ spectrum and $OD(\omega)$ spectrum for large number of different static disorder realizations created by random number generator. Finally these results have to be averaged over all realizations of static disorder. Time evolution of exciton density matrix has to be calculate also for each realization of static disorder. That is why it was necessary to put through numerical integrations for each realization of static disorder (see (14)).

For the most of our calculations the software package *Mathematica* [27] was used. This package is very convenient and has very wide range of applications in different areas of research [28]–[30] not only for symbolic calculations [31] which are needed for expression of all required quantities, but it can be used also for numerical ones [32]. That is why the software package *Mathematica* was used by us as for symbolic calculations as for numerical integrations and also for final averaging of results over all realizations of static disorder.

As concerns the time development of our system, for the solution of the Redfield equation we have used the program written in Fortran and standard Runge-Kutta method.

IV. RESULTS

Three above mentioned types of uncorrelated static disorder have been taken into account in our simulations simultaneously with dynamic disorder in Markovian approximation. Dimensionless energies normalized to the

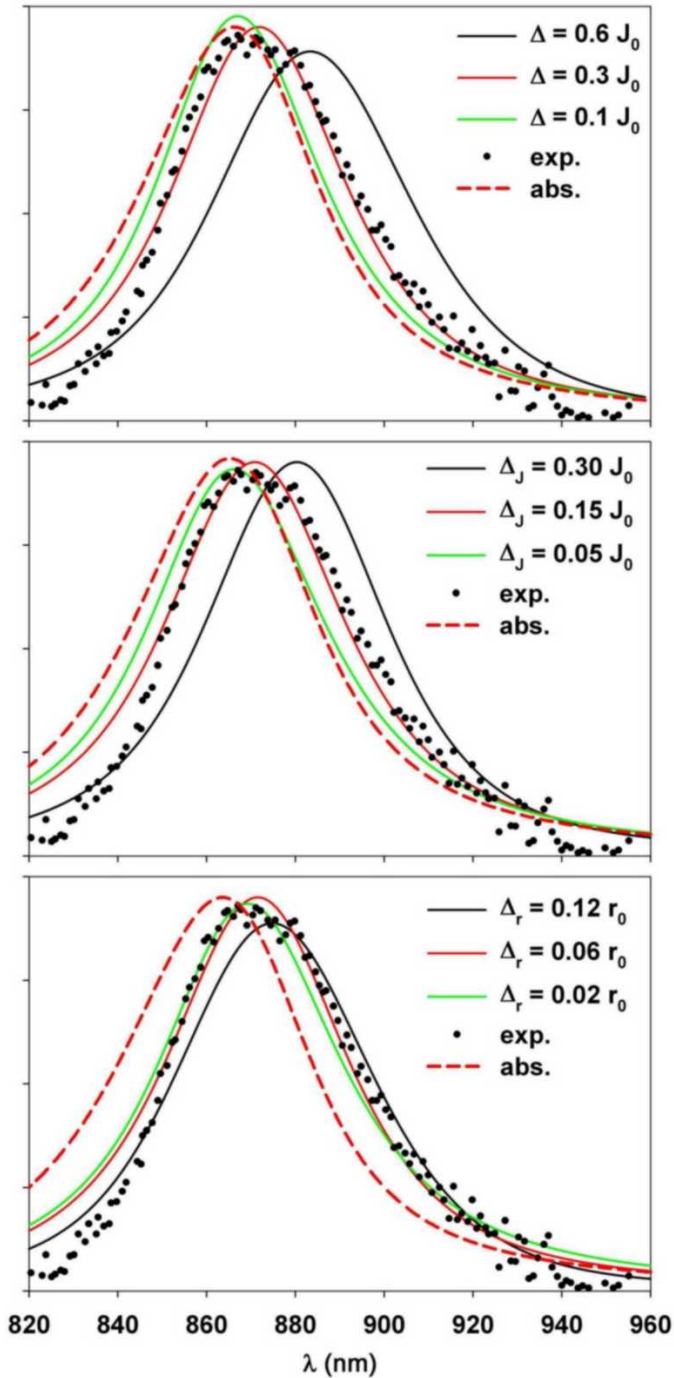


Fig. 1. Resulting absorption $OD(\omega)$ (dashed lines) and steady-state fluorescence $FL(\omega)$ spectra (solid lines) of LH2 at room temperature $kT = 0.5 J_0$ for three different types and three different strengths of static disorder, averaged over 2000 realizations: First row - Gaussian uncorrelated disorder in local excitation energies $\delta\varepsilon$, second row - Gaussian uncorrelated static disorder in nearest neighbour transfer integrals δJ , third row - Gaussian uncorrelated static disorder in radial positions of molecules δr . Experimental fluorescence profile averaged in time and over the particles for room temperature is also displayed (points).

transfer integral $J_{12} = J_0$ and dimensionless time τ have been used. Estimation of J_0 varies in literature between

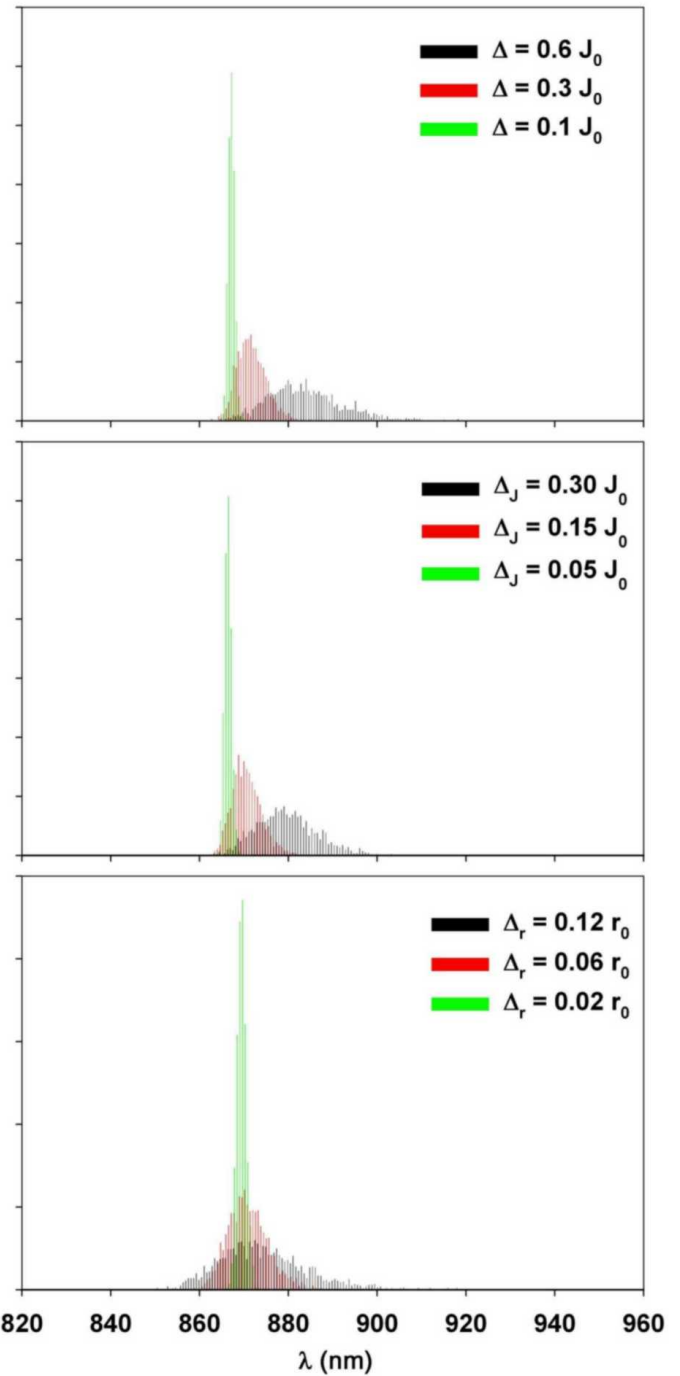


Fig. 2. Peak position distributions of calculated steady-state single ring fluorescence spectra $FL(\omega)$ of LH2 at room temperature $kT = 0.5 J_0$ for 2000 realizations of static disorder for three different types and three different strengths of static disorder: First row - Gaussian uncorrelated static disorder in local excitation energies $\delta\varepsilon$, second row - Gaussian uncorrelated static disorder in nearest neighbour transfer integrals δJ , third row - Gaussian uncorrelated static disorder in radial positions of molecules δr .

250 cm^{-1} and 400 cm^{-1} . For these extreme values of J_0 our time unit ($\tau = 1$) corresponds to 21.2 fs or 13.3 fs.

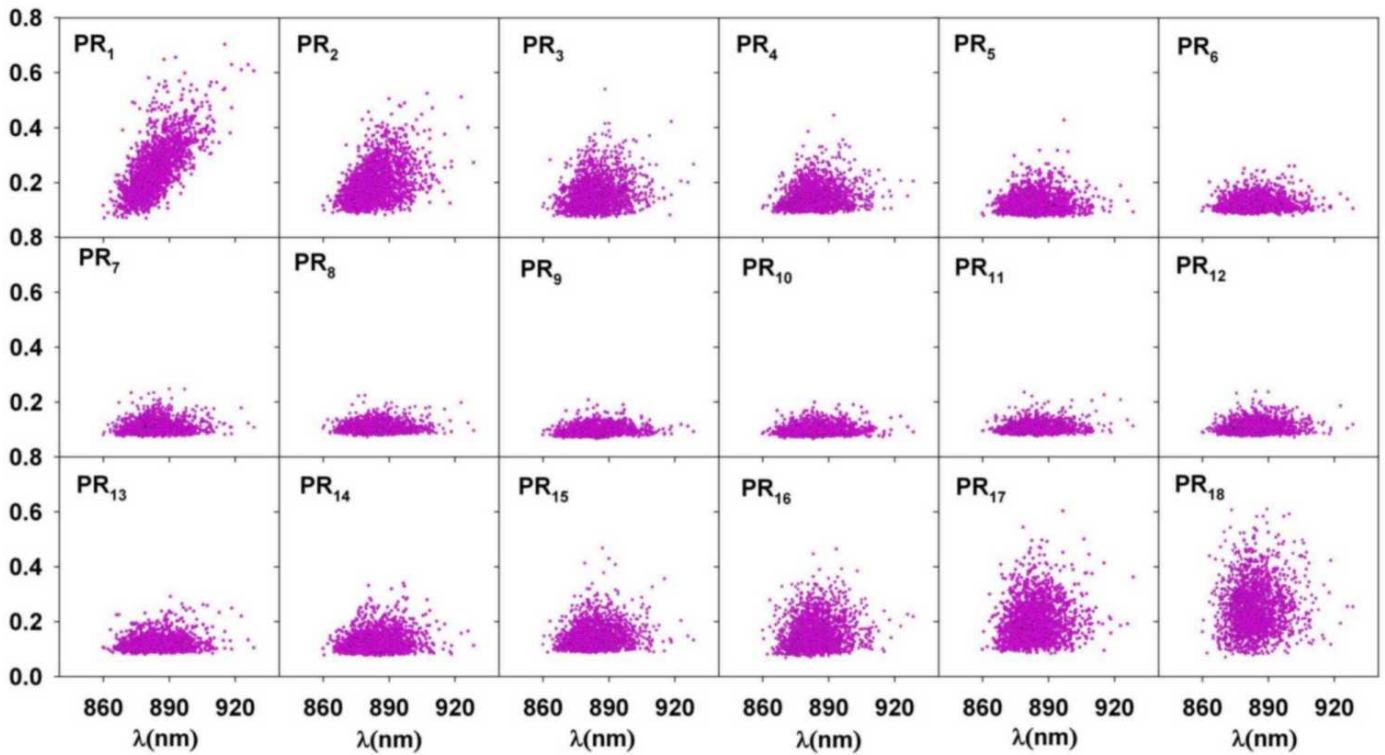


Fig. 3. The distributions of PR_α values ($\alpha = 1, \dots, 18$) as a function of FL spectrum peak position at room temperature $kT = 0.5 J_0$ calculated for 2000 realizations of Gaussian uncorrelated static disorder in local excitation energies $\delta\varepsilon$, $\Delta = 0.6 J_0$.

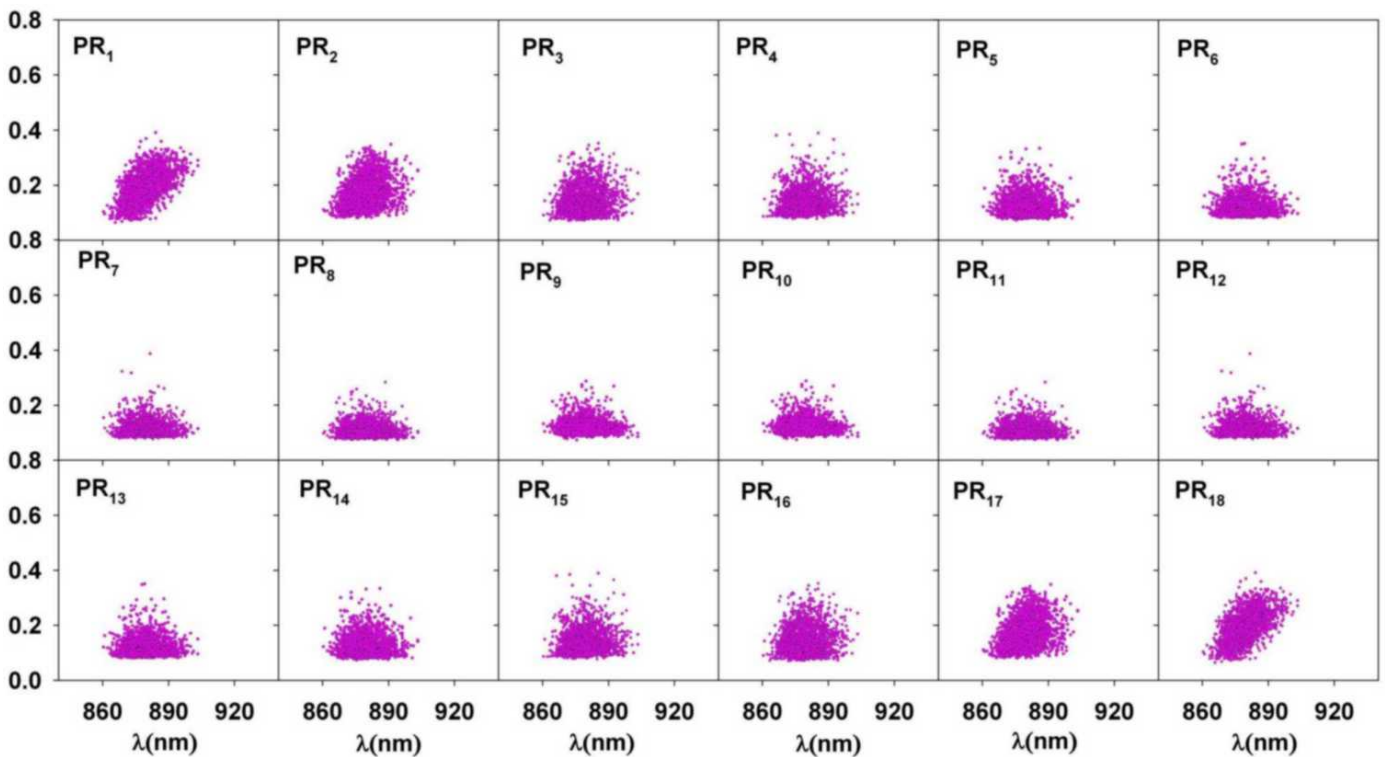


Fig. 4. The distributions of PR_α values ($\alpha = 1, \dots, 18$) as a function of FL spectrum peak position at room temperature $kT = 0.5 J_0$ calculated for 2000 realizations of Gaussian uncorrelated static disorder in nearest neighbour transfer integrals δJ_{mn} , $\Delta_J = 0.30 J_0$.

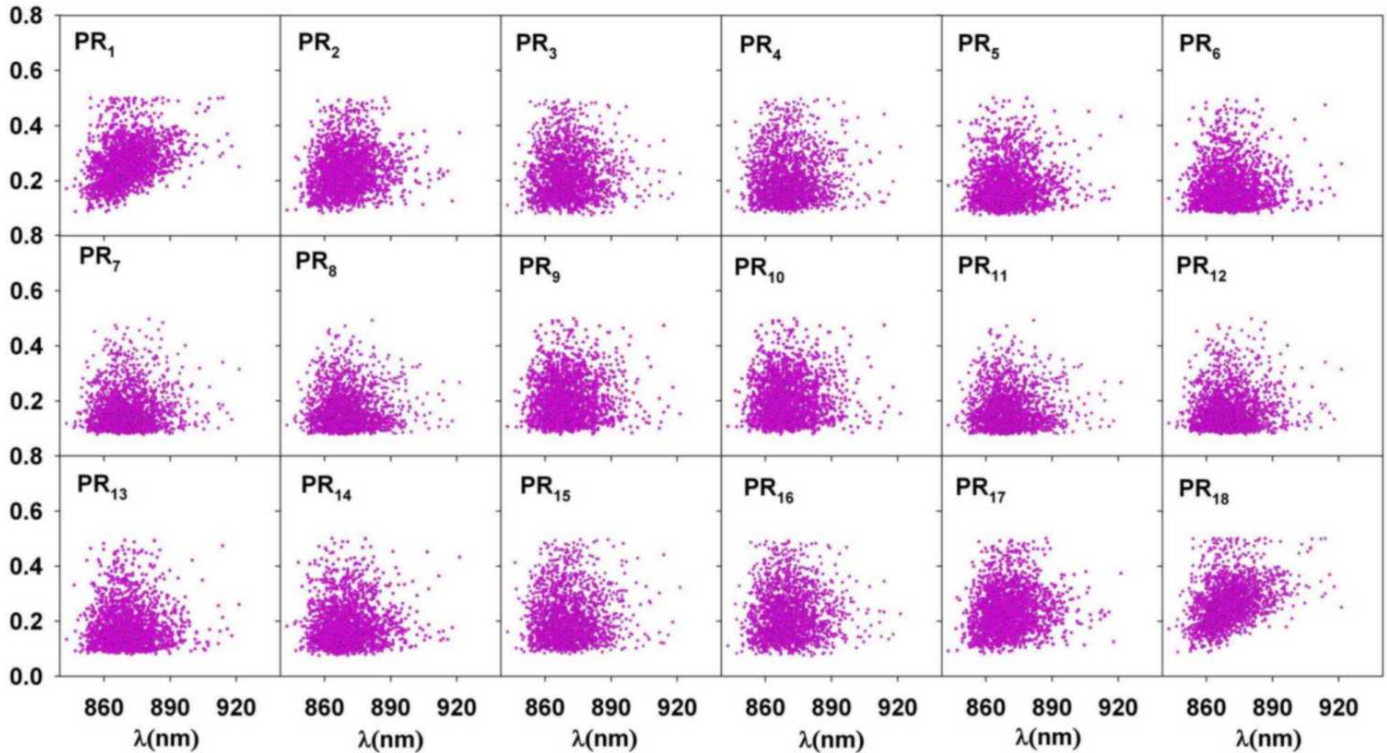


Fig. 5. The distributions of PR_α values ($\alpha = 1, \dots, 18$) as a function of FL spectrum peak position at room temperature $kT = 0.5 J_0$ calculated for 2000 realizations of Gaussian uncorrelated static disorder in radial positions of molecules on the ring δr_n , $\Delta_r = 0.12 r_0$.

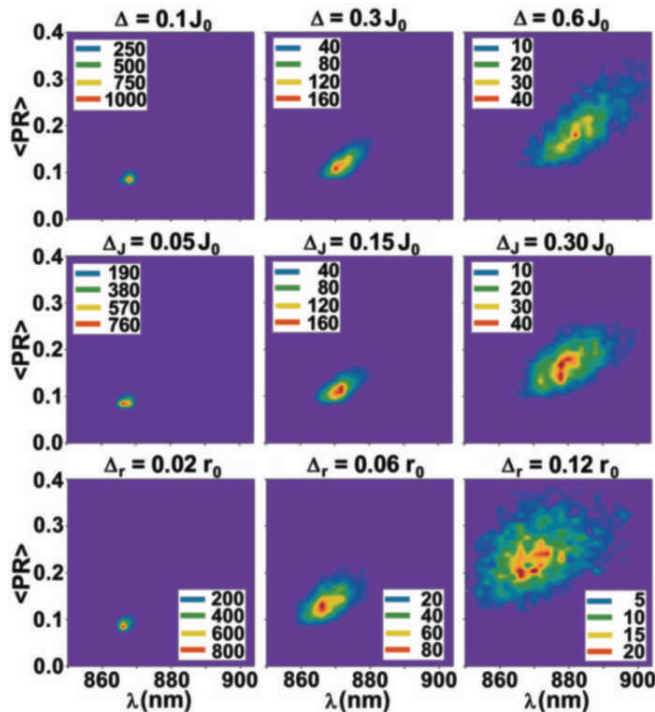


Fig. 6. The distribution of $\langle PR \rangle$ values as a function of FL spectrum peak position at room temperature $kT = 0.5 J_0$ calculated for 2000 realizations of Gaussian uncorrelated static disorder: in local excitation energies $\delta\epsilon$ (first row), in nearest neighbour transfer integrals δJ (second row), in radial positions of molecules δr (third row). Columns: three different strengths of static disorder.

Contrary to Novoderezhkin et al. [19] different model of spectral density (the model of Kühn and May [12]) has been used. In agreement with our previous results [33] we have used the strength of dynamic disorder $j_0 = 0.4 J_0$ and cut-off frequency $\omega_c = 0.212 J_0$ (see (21)).

The strengths of individual types of uncorrelated static disorder have been taken in agreement with [34]. For each type of static disorder the simulations have been done for three values of the static disorder strength:

- (I) $\Delta = 0.1, 0.3, 0.6 J_0$,
- (II) $\Delta_J = 0.05, 0.15, 0.30 J_0$,
- (III) $\Delta_r = 0.02, 0.06, 0.12 r_0$, where r_0 is the radius of unperturbed ring.

Resulting absorption $OD(\omega)$ and steady state fluorescence spectra $FL(\omega)$ for room temperature $kT = 0.5 J_0$ averaged over 2000 realizations of each static disorder type and strength can be seen in Fig. 1. Comparison of calculated FL spectra with experimental FL profile averaged in time and over the particles [19] is also displayed in Fig. 1.

Fig. 2 presents the peak positions distributions of calculated steady state single ring fluorescence spectra at room temperature $kT = 0.5 J_0$ for 2000 realizations of static disorder. The distributions are shown for three types and three strengths of static disorder mentioned above.

The distributions of the participation ratios PR_α for

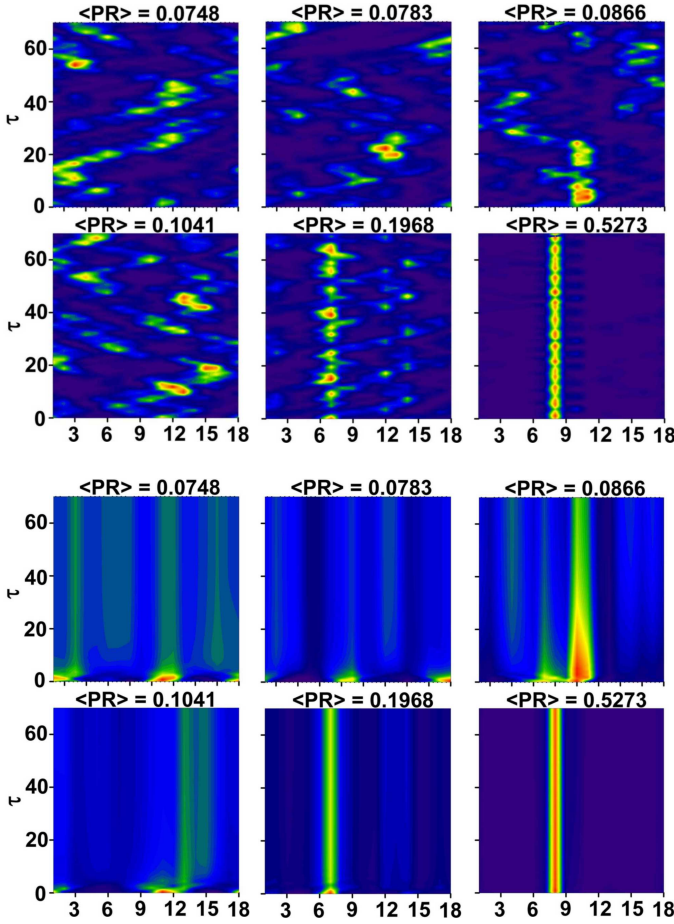


Fig. 7. The diagonal exciton density matrix elements in the site representation ρ_{nn} at room temperature ($kT = 0.5J_0$) are shown as a function of time τ for Gaussian uncorrelated static disorder type (I) - fluctuations of local excitation energies $\delta\varepsilon_n$. First and second row shows the coherent dynamics (without dynamic disorder) for the realizations of static disorder with lowest (first row) and highest (second row) $\langle PR \rangle$ values. The third and fourth row shows the same but with the dynamic disorder effect taking into account. Columns: three different strengths of static disorder.

each of eighteen eigenstates α can be seen in Fig. 3 - Fig. 5 for highest strength of each static disorder type ($\Delta = 0.6 J_0$, $\Delta_J = 0.30 J_0$, $\Delta_r = 0.12 r_0$).

Fig. 6 shows the values of thermally averaged participation ratio $\langle PR \rangle$ as a function of FL spectrum peak position at room temperature $kT = 0.5 J_0$ calculated for 2000 realizations of the disorder.

Dynamics of the diagonal exciton density matrix elements in site representation ρ_{nn} is shown in Fig. 7 - 9 for three above mentioned static disorder types. Initial density matrix $\rho_{\alpha\beta}(t=0)$ is chosen by us corresponding to coherent wavepacket with steady state populations P_α and arbitrary fixed phases φ_α [19],

$$\rho_{\alpha\beta} = \sqrt{P_\alpha P_\beta} e^{i(\varphi_\alpha - \varphi_\beta)}, \quad (26)$$

and

$$\rho_{\alpha\alpha} = P_\alpha \sim e^{-\frac{\varepsilon_\alpha}{kT}}. \quad (27)$$

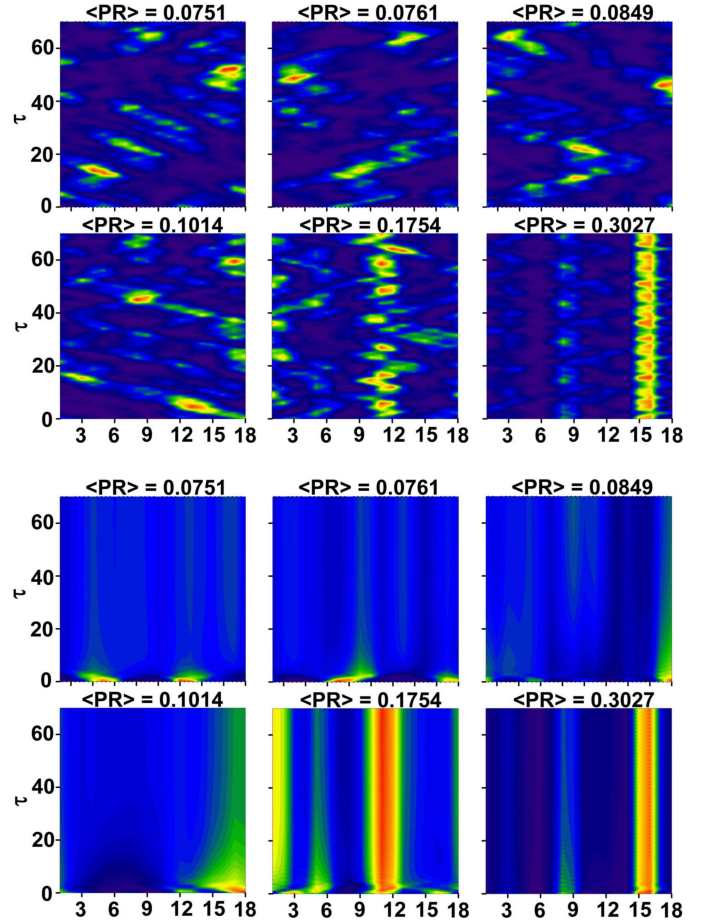


Fig. 8. The diagonal exciton density matrix elements in the site representation ρ_{nn} at room temperature ($kT = 0.5J_0$) are shown as a function of time τ for Gaussian uncorrelated static disorder type (II) - fluctuations of nearest neighbour transfer integrals δJ_{mn} . First and second row shows the coherent dynamics (without dynamic disorder) for the realizations of static disorder with lowest (first row) and highest (second row) $\langle PR \rangle$ values. The third and fourth row shows the same but with the dynamic disorder effect taking into account. Columns: three different strengths of static disorder.

Timescale $\tau \in \langle 0; 70 \rangle$ corresponds to $t \in (0; 1.4 \text{ ps})$ or $(0; 1 \text{ ps})$ for limit values of J_0 mentioned above. Initial exciton density matrix is defined as follows: initial populations in eigenstate representation ($\rho_{\alpha\alpha}$) correspond to a thermally equilibrated wavepacket at room temperature ($kT = 0.5 J_0$), initial coherences ($\rho_{\alpha\beta}$, $\alpha \neq \beta$) have arbitrary fixed phases. Contrary to [19] the dynamic disorder have been taken into account in our simulations. First and second rows of Fig. 7 - 9 show the coherent dynamics (without dynamic disorder) for the realizations of static disorder with lowest and highest $\langle PR \rangle$ values. The third and fourth rows show the same but with the dynamic disorder effect taking into account.

V. CONCLUSION

Software package *Mathematica* has been found by us very useful for the simulations of the spectra of molecular

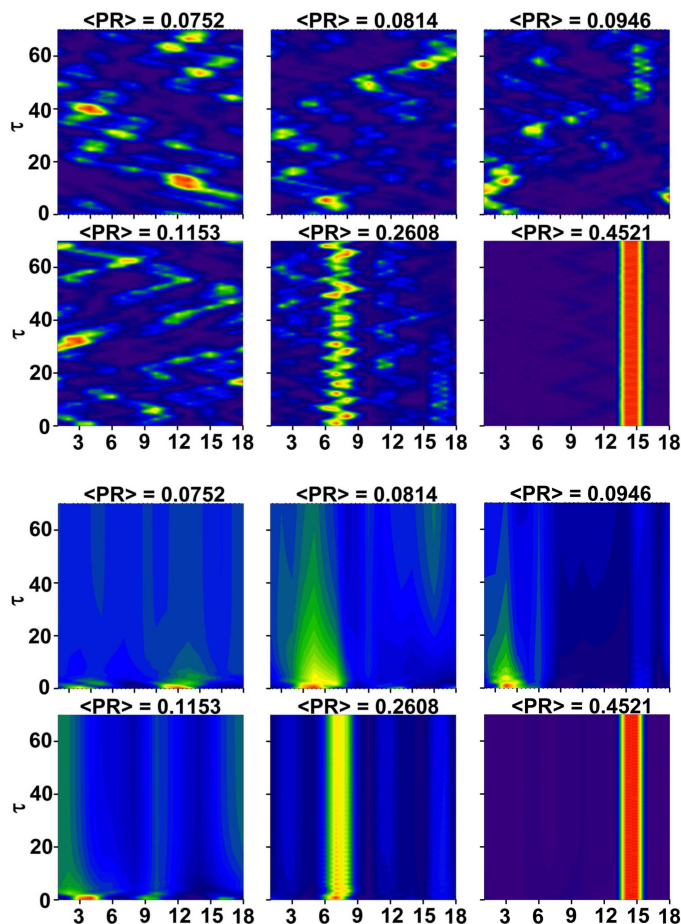


Fig. 9. The diagonal exciton density matrix elements in the site representation ρ_{nn} at room temperature ($kT = 0.5J_0$) are shown as a function of time τ for Gaussian uncorrelated static disorder type (III) - fluctuations of radial positions of molecules δr_n on the ring. First and second row shows the coherent dynamics (without dynamic disorder) for the realizations of static disorder with lowest (first row) and highest (second row) $\langle PR \rangle$ values. The third and fourth row shows the same but with the dynamic disorder effect taking into account. Columns: three different strengths of static disorder.

rings. From the comparison of our simulated FL spectra with experimental data (Fig. 1) the values of the inter-pigment interaction energy J_0 and unperturbed transition energy from the ground state ΔE_0 were obtained [35].

The fluorescence spectra shift to higher wavelengths (to lower energies) for increasing static disorder (it can be seen from Fig. 1). This shift is the smallest in case of static disorder in radial positions of molecules (III).

In Fig. 1 the shift of fluorescence spectra peak position to the higher wavelength in comparison with absorption spectra peak position is also visible. This shift is highest (8 nm) for the static disorder type (III).

The differences in localization of eigenstates α for different types of static disorder we can see in Fig. 3 - 5. In case of the static disorder type (III), the dispersions of PR_α values are almost the same for all eigenstates α (Fig. 5). However, in case of static disorder types (I) and

(II), larger differences in dispersion are visible (Fig. 3 and 4). For these types of static disorder the dispersions are much larger for the lowest and highest eigenstates in comparison with intermediate ones.

From Figure 6 it can be seen growing of $\langle PR \rangle$ values in case of higher strength of static disorder. It corresponds to more localized exciton states. Shift to lower wavelengths is evident for the static disorder type (III) in comparison with other static disorder types.

From Fig. 7 - 9 no significant difference in exciton density matrix dynamics for different types of static disorder is visible. Different degree of localization $\langle PR \rangle$ produce different types of coherent excitation dynamics. The population distribution for small $\langle PR \rangle$ is more or less uniform, i.e., excitation can be found on any part of the ring. The wavepacket moves around the ring in this case. On the other hand, higher values of $\langle PR \rangle$ lead to higher localization of excitation on a smaller group of pigments or even on a single pigment. Excitation can be even totally localized on a single molecule without any migration to the other sites in case of highest $\langle PR \rangle$. If the dynamic disorder is taken into account, oscillations in exciton dynamics are suppressed. The dynamics can be characterized by relaxation.

REFERENCES

- [1] G. McDermott et al., Crystal-structure of an integral membrane light-harvesting complex from photosynthetic bacteria, *Nature* 374, 1995, pp. 517-521.
- [2] M. Z. Papiz et al., The structure and thermal motion of the B800-850 LH2 complex from *Rps. acidophila* at 2.0 Å over-circle resolution and 100 K: New structural features and functionally relevant motions, *J. Mol. Biol.* 326, 2003, pp. 1523-1538.
- [3] R. Kumble, R. Hochstrasser, Disorder-induced exciton scattering in the light-harvesting systems of purple bacteria: Influence on the anisotropy of emission and band \rightarrow band transitions, *J. Chem. Phys.* 109, 1998, pp. 855-865.
- [4] V. Nagarajan et al., Ultrafast exciton relaxation in the B850 antenna complex of *Rhodobacter sphaeroides*, *Proc. Natl. Acad. Sci. USA* 93, 1996, pp. 13774-13779.
- [5] V. Nagarajan et al., Femtosecond pump-probe spectroscopy of the B850 antenna complex of *Rhodobacter sphaeroides* at room temperature, *J. Phys. Chem. B* 103, 1999, pp. 2297-2309.
- [6] V. Nagarajan, W. W. Parson, Femtosecond fluorescence depletion anisotropy: Application to the B850 antenna complex of *Rhodobacter sphaeroides*, *J. Phys. Chem. B* 104, 2000, pp. 4010-4013.
- [7] V. Čápek, I. Barvík, P. Heřman, Towards proper parametrization in the exciton transfer and relaxation problem: dimer, *Chem. Phys.* 270, 2001, pp. 141-156.
- [8] P. Heřman, I. Barvík, Towards proper parametrization in the exciton transfer and relaxation problem. II. Trimer, *Chem. Phys.* 274, 2001, pp. 199-217.
- [9] P. Heřman, I. Barvík, M. Urbanec, Energy relaxation and transfer in excitonic trimer, *J. Lumin.* 108, 2004, pp. 85-89.
- [10] P. Heřman et al., Exciton scattering in light-harvesting systems of purple bacteria, *J. Lumin.* 94-95, 2001, pp. 447-450.
- [11] P. Heřman, I. Barvík, Non-Markovian effects in the anisotropy of emission in the ring antenna subunits of purple bacteria photosynthetic systems, *Czech. J. Phys.* 53, 2003, pp. 579-605.
- [12] P. Heřman et al., Influence of static and dynamic disorder on the anisotropy of emission in the ring antenna subunits of purple bacteria photosynthetic systems, *Chem. Phys.* 275, 2002, pp. 1-13.
- [13] P. Heřman, I. Barvík, Temperature dependence of the anisotropy of fluorescence in ring molecular systems, *J. Lumin.* 122-123, 2007, pp. 558-561.

- [14] P. Heřman, I. Barvík, Coherence effects in ring molecular systems, *Phys. Stat. Sol. C* 3, 2006, 3408-3413.
- [15] P. Heřman, D. Zapletal, I. Barvík, The anisotropy of fluorescence in ring units III: Tangential versus radial dipole arrangement, *J. Lumin.* 128, 2008, pp. 768-770.
- [16] P. Heřman, I. Barvík, D. Zapletal, Computer simulation of the anisotropy of fluorescence in ring molecular systems: Tangential vs. radial dipole arrangement, *Lecture Notes in Computer Science* 5101, 2008, pp. 661-670.
- [17] P. Heřman, D. Zapletal, J. Šlégr, Comparison of emission spectra of single LH2 complex for different types of disorder, *Physics Procedia* 13, 2011, pp. 14-17.
- [18] D. Zapletal, P. Heřman, Computer simulation of fluorescence spectra for molecular ring: exciton dynamics, in *Proceedings of the 13th WSEAS International Conference on Mathematical and Computational Methods in Science and Engineering (MACMESE '11)* WSEAS Press, 2011, pp. 182-187.
- [19] V. I. Novoderezhkin, D. Rutkauskas, R. van Grondelle, Dynamics of the emission spectrum of a single LH2 complex: Interplay of slow and fast nuclear motions, *Biophys. J.* 90, 2006, pp. 2890-2902.
- [20] W. M. Zhang et al., Exciton-migration and three-pulse femtosecond optical spectroscopies of photosynthetic antenna complexes, *J. Chem. Phys.* 108, 1998, pp. 7763-7774.
- [21] S. Mukamel, *Principles of nonlinear optical spectroscopy*. New York: Oxford University Press, 1995.
- [22] A. G. Redfield, The Theory of Relaxation Processes, *Adv. Magn. Reson.* 1, 1965, pp. 1-32.
- [23] D. Rutkauskas et al., Fluorescence spectroscopy of conformational changes of single LH2 complexes, *Biophys. J.* 88, 2005, pp. 422-435.
- [24] D. Rutkauskas et al., Fluorescence spectral fluctuations of single LH2 complexes from *Rhodospseudomonas acidophila* strain 10050, *Biochemistry* 43, 2004, pp. 4431-4438.
- [25] V. May, O. Kühn, *Charge and Energy Transfer in Molecular Systems*. Berlin: Wiley-WCH, 2000.
- [26] O. Zerlauskienė et al., Static and Dynamic Protein Impact on Electronic Properties of Light-Harvesting Complex LH2, *J. Phys. Chem. B* 112, 2008, pp. 15883-15892.
- [27] S. Wolfram, *The Mathematica Book*, 5th ed., Wolfram Media, 2003.
- [28] A. A. Keller, Genetic Search Algorithms to Fuzzy Multiobjective Games: A Mathematica Implementation, in *10th WSEAS International Conference on Applied Computer Science*, Athens, 2010, pp. 351-359.
- [29] D. Ustundag, M. Cevri, Bayesian Parameter Estimation of Sinusoids with Simulated Annealing, in *8th WSEAS International Conference on Signal Processing, Computational Geometry and Artificial Vision*, Athens, 2008, pp. 106-112.
- [30] M. C. Voicu, Computational Methods and Analytical Study for Detecting the Attractors of a Particular Type of k-Order, Nonlinear, Exchange Rate Models, in *13th WSEAS International Conference on Computers*, Athens, 2009, pp. 289-302.
- [31] M. Trott, *The Mathematica GuideBook for Symbolics*. New York: Springer Science+Business Media, Inc., 2006.
- [32] M. Trott, *The Mathematica GuideBook for Numerics*. New York: Springer Science+Business Media, Inc., 2006.
- [33] P. Heřman, D. Zapletal, I. Barvík, Computer simulation of the anisotropy of fluorescence in ring molecular systems: Influence of disorder and ellipticity, in *Proc. IEEE 12th International Conference on Computational Science and Engineering (CSE '09)*, Vancouver, 2009, pp. 437-442.
- [34] P. Heřman, I. Barvík, D. Zapletal, Energetic disorder and exciton states of individual molecular rings, *J. Lumin.* 119-120, 2006, pp. 496-503.
- [35] P. Heřman, D. Zapletal, M. Horák, Computer simulation of steady state emission and absorption spectra for molecular ring, in *Proc. 5th International Conference on Advanced Engineering Computing and Applications in Sciences (ADVCOMP2011)*, Lisbon, 2011, accepted.